# Nanofabrication and electrostatic operation of single-crystal silicon paddle oscillators

S. Evoy,[a] D. W. Carr, L. Sekaric, A. Olkhovets, J. M. Parpia, and H. G. Craighead
*Cornell Center for Materials Research and Cornell Nanofabrication Facility, Clark Hall, Cornell University, Ithaca, New York 14853*

(Received 10 May 1999; accepted for publication 1 September 1999)

We report the fabrication and characterization of paddle oscillators featuring nanometer-scale supporting rods. The devices show two resonances in the 1–10 MHz range, which we attribute to the translational and torsional modes of motion. While the frequency response of the translational motion shows evidence of nonlinear behavior, the torsional response remains symmetric throughout the range of excitation. We present a model for the electrostatic excitation of the two modes. Torsional motion is induced via asymmetries of the system, and amplified by a modulation of the effective torsional constant. The model of the translational motion predicts a nonlinear behavior for displacements as small as 15 nm. Analysis of both modes of motion consistently suggests structures softer than expected from bulk silicon. Quality factors approaching $10^3$ are measured. © *1999 American Institute of Physics.* [S0021-8979(99)06923-6]

## I. INTRODUCTION

Nanoelectromechanical systems (NEMS) are of interest from both scientific and technological standpoints. Micromechanical devices are commonly employed in an increasingly broad range of consumer and scientific applications such as ink jet printing, automobile safety devices, and probe microscopy. Torque magnetometry has been performed with macroscopic single-crystal silicon resonators.[1–4] Smaller structures are being considered for use as chemical sensors, force gauges,[5,6] nano-actuators,[7] magnetic resonance force microscopes,[8] and for various optomechanical and biomedical applications. Small resonant structures also open fascinating avenues for mesoscopic studies of the mechanical properties of materials,[9–12] and of interesting parametric amplification effects.[13,14]

We have recently reported the fabrication and excitation of released Si structures with lateral dimensions as small as 30 nm.[15] This technology has been applied for the fabrication and operation of devices at frequencies as high as 380 MHz.[16] In this article we report the fabrication and characterization of paddle oscillators with nanometer-scale supporting rods. Paddle oscillators of such dimensions have recently been proposed as torsional mechanical electrometers.[17] This last study involved electromagnetic excitation and detection of the devices, and required intense magnetic fields at low temperature. Here we report on the fabrication of electrostatically-driven oscillators that are detected at room temperature using an optical modulation technique.[9,15,18] We also model and experimentally characterize the electrostatic excitation and response of the devices, and demonstrate the ability of this optical scheme to detect motion in the angstrom range.

[a]Electronic mail: se20@cornell.edu

## II. EXPERIMENTAL

The fabrication process has been described previously.[15] Devices are produced on silicon-on-insulator wafers consisting of a 400-nm-thick oxide buried underneath 200 nm of single-crystal (100) silicon. A Cr etch mask is first defined using electron beam lithography, thermal evaporation, and lift-off. Pattern is transferred through the top silicon layer using a $CF_4/H_2$ reactive ion etch. Structures are released by undercutting through the buried oxide layer by wet hydrofluoric acid etch. Two independent top-surface electrical contact planes are formed at the top and bottom Si layers by evaporating thin layers of Cr (3 nm) and Au (17 nm) on the entire surface.

Devices are operated in a small vacuum chamber pumped down to the $10^{-4}$ Torr range. The tracking output of a Hewlett Packard ESA-L1500A spectrum analyzer provides a driving rf signal. As discussed later, a dc offset is added to the rf signal in order to linearize the voltage dependence of the driving force. The plane of the underlying surface is grounded. Motion is detected using an optical modulation technique.[9,15,18] A He–Ne laser is focused onto the paddle using a 0.35 numerical aperture (NA) microscope objective. The motion of the paddle modulates the reflected signal through interferometric effects.[15] Modulation of the reflected laser beam is detected by a New Focus 1601 ac coupled photodetector, whose output is fed to the input of the spectrum analyzer. The relationship between the detected signal and the amplitude of motion is discussed later.

A typical device is shown in Fig. 1. All experiments described here are performed on paddles supported by beams of length $L=2.5\mu$m and width $b=175$ nm. Thickness of the wires and paddle is fixed at $a=200$ nm by the initial thickness of the top silicon layer. The paddle width is maintained at $w=2\mu$m. However, paddle length is varied from $d=2$ to 5 $\mu$m to allow the experimental verification of parameter-dependent terms in our models. The paddle is suspended at

 

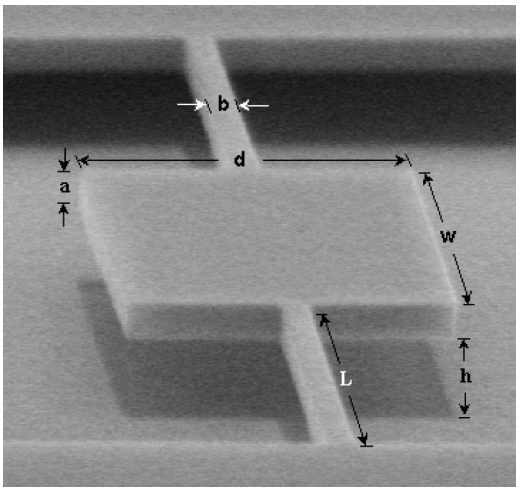


FIG. 1. Scanning electron micrograph of a nanofabricated paddle oscillator. $a=200$, $b=175$ nm, $d=2.5$ $\mu$m, $w=2$ $\mu$m, $h=400$ nm, $L=2.5$ $\mu$m.

$h=400$ nm above the bottom silicon surface, as fixed by the original thickness of the buried oxide.

## III. EXPERIMENTAL IDENTIFICATION OF MODES OF MOTION

Operation of devices reveals the presence of two resonant frequencies in the 1–10 MHz range. Their different behavior under increased drive amplitude (Fig. 2) suggests their association with two different types of motion. The two resonant frequencies are therefore preliminary attributed to the excitation of translational and torsional modes of motion, respectively (Fig. 3). This attribution is experimentally verified by taking advantage of the different length dependence of the inertia associated with each mode

$$f_0^{\text{translational}}=\frac{1}{2\pi}\sqrt{\frac{k}{M}}\propto d^{-0.5}, \tag{1a}$$

$$f_0^{\text{torsional}}=\frac{1}{2\pi}\sqrt{\frac{\kappa}{I}}\propto d^{-1.5}, \tag{1b}$$

where $k$ and $\kappa$ are linear restoring constants for the translational and torsional modes, respectively, $d$ is the paddle length, $M$ is its mass, and $I$ is its inertia. We have measured the frequency of both resonances for a series of eight devices of varying paddle length (Fig. 4). A fit of data of a $f=Kd^b$ power law reveals experimental power coefficients of $b_1=-0.5\pm0.1$ and $b_2=-1.6\pm0.15$, respectively. These coefficients are in agreement with the values expected from Eqs. (1), confirming the respective translational and torsional nature of the two resonant frequencies.

The detected optical amplitude for the torsional motion increases linearly with the rf voltage [Fig. 2(b)]. As expected from small displacements, this finding supports a linear relationship between the drive amplitude, the resulting oscillation, and the observed modulation of the reflected signal over the range of motion. Furthermore, while the torsional mode peak remains symmetric [Fig. 2(b)] throughout the range of applied torques, nonlinear behavior is observed for the translational motion [Fig. 2(a)] even at the lowest drive amplitudes. We present models for the two modes of motion, and discuss their experimentally observed behavior. While the translational analysis concentrates on nonlinear behavior, the torsional analysis focuses on the modulation of the effective torsional constant and its related effects.

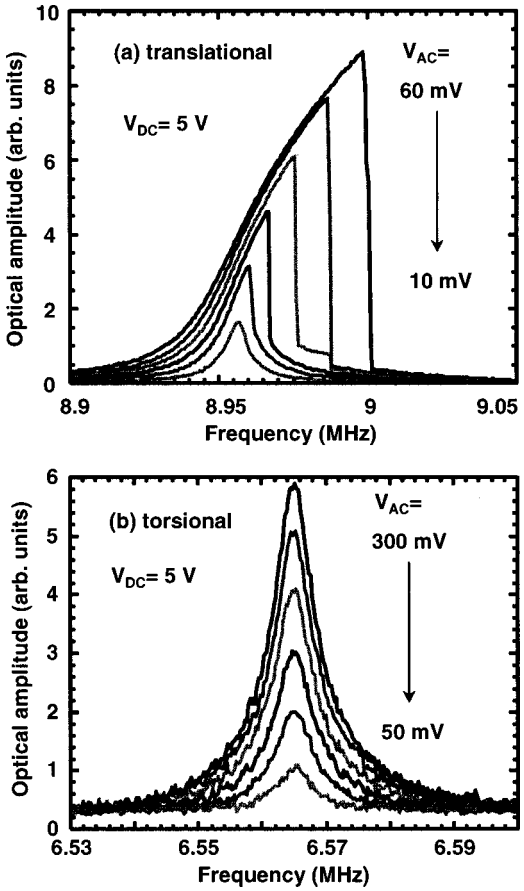


FIG. 2. Observed translational and torsional resonant responses of a paddle oscillator of $d=3$ $\mu$m.

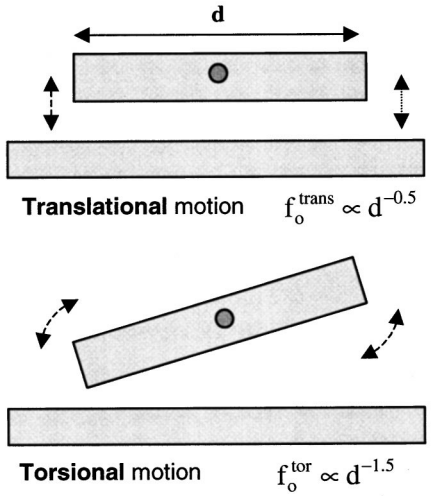


FIG. 3. Schematic diagrams of translational and torsional motion.

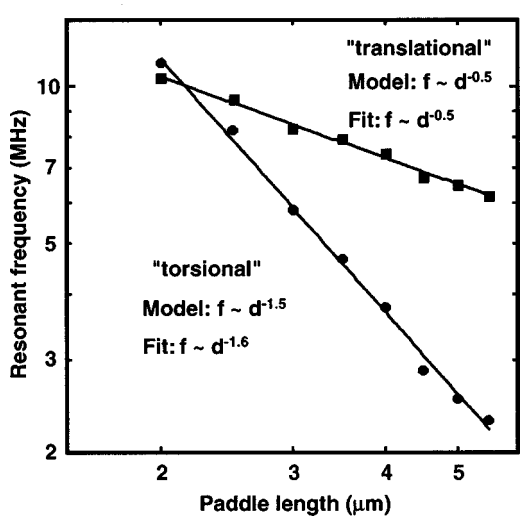


FIG. 4. Dependence of resonant frequency on paddle length for translational and torsional motion.

## IV. CHARACTERIZATION OF TRANSLATIONAL MOTION

The modeling of the translational mode begins with an equation of motion of a damped oscillator

$$\ddot{\delta}+K_1\delta+K_3\delta^3+\frac{1}{\omega_0 Q}\dot{\delta}=\frac{F(\omega t)}{M}, \tag{2}$$

where $\delta$ is a small displacement in the vertical direction, $M$ is the total mass of paddle and metal layers, and $F$ is the external force. Damping is expressed through the quality factor $Q$ of the structure. Nonlinearity is introduced with a cubic force constant $K_3$.

The linear restoring constant is evaluated by considering the deflection of a beam clamped at one end.[19]

$$F_z=\frac{Ea^3b}{4L^3}\,\delta_{\text{one end}}, \tag{3}$$

where $E$ is Young's modulus of bulk silicon. As a result of the high rigidity of the paddle, we consider each beam to be clamped at both ends (Fig. 5). From symmetry arguments, the point halfway along each beam will not be bent, and is therefore under no flexural tension. This halfway point is therefore considered as the joining point of two half-length beams clamped only at their opposite extremity. The deflection of each half-length beam is half the total deflection of the entire beam. Introducing these arguments, we obtain

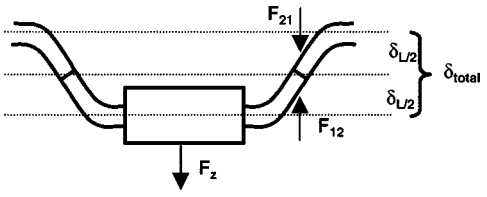


FIG. 5. Schematic diagram of a paddle oscillator displaced by a force $F_z$. Each beam is clamped at both ends. Given that the middle point is under no flexural tension, each beam is approximated by two half-length beams clamped on one end only. Under a force of $F_{12}=F_{21}=F_z$, each half-length beam is displaced by $\delta_{L/2}=\delta_{\text{total}}/2$.

$$F_z=\frac{Ea^3b}{4(L/2)^3}\,\frac{\delta_{\text{total}}}{2}, \tag{4}$$

where we have used Eq. (3) with $L/2\rightarrow L$, and $\delta_{L/2}=\delta_{\text{total}}/2$. Finally, the beams from both sides of the paddle add up to a total linear restoring term of

$$K_1=2\,\frac{Ea^3b}{ML^3}. \tag{5}$$

In the absence of nonlinear effects, this expression also provides the expected linear resonant frequency of the translational motion

$$f_0=\frac{1}{2\pi}\sqrt{2\,\frac{Ea^3b}{ML^3}}. \tag{6}$$

The nonlinear effects induced by beam stretching are introduced using textbook approaches of suspended power lines and bridge cables.[20] When the paddle is moved from its rest position, the total length of the supporting beams must change to accommodate the displacement. We approximate that the beams remain straight while being stretched down to an angle $\phi$. The restoring force provided by this stretching is

$$F=\epsilon Eab\phi, \tag{7}$$

where $\epsilon$ is the strain in the beam, $ab$ is the cross-sectional area of the beam, and $\phi$ is its angular displacement. The strain is computed from geometrical arguments

$$\epsilon=\frac{\Delta L}{L}=\frac{(L+\Delta L)-L}{L}$$
$$=\frac{L\left(\frac{1}{\cos\phi}-1\right)}{L}\approx\frac{1}{\sqrt{1-\phi^2}}-1\approx\frac{\phi^2}{2}, \tag{8}$$

which we replace in Eq. (7)

$$F_3=Eab\,\frac{\phi^3}{2}. \tag{9}$$

Given that $\delta\sim\phi L$, we obtain

$$K_3=\frac{Eab}{2ML^3}. \tag{10}$$

The remaining component of the equation of motion is the right-hand drive term. Electrostatic forces that depend on the square of the applied voltage drive the device

$$F(\omega t)=\frac{\epsilon_0 wd}{h^2}V^2(\omega t). \tag{11}$$

The presence of the paddle-surface distance $h$ in Eq. (11) would represent a displacement dependence of the driving force. However, we consider the vertical displacement $\delta$ to be small compared to the average height $h$, and neglect its contribution to Eq. (11).

The force therefore depends on the square of the applied voltage. A dc bias ($V_{\text{dc}}\gg V_{\text{ac}}$) is added to the rf signal in order to force a linear cross term

$$V^2(\omega t)=[V_{dc}+V_{ac}\cos(\omega t)]^2$$
$$=V_{dc}^2+2V_{dc}V_{ac}\cos(\omega t)+V_{ac}^2\cos^2(\omega t). \quad (12)$$

The equation of motion becomes

$$\ddot{\delta}+K_1\delta+K_3\delta^3+\frac{1}{\omega_0 Q}\dot{\delta}$$
$$=\frac{\epsilon_0 wd}{Mh^2}[V_{dc}^2+2V_{dc}V_{ac}\cos(\omega t)+V_{ac}^2\cos^2(\omega t)]. \quad (13)$$

Assuming a solution of the form[21]

$$\delta=\frac{1}{\sqrt{2K_1}}[Ae^{-i\omega t}+A^*e^{i\omega t}] \quad (14)$$

and keeping only the terms in $e^{-i\omega t}$, we find

$$\left[\frac{3K_3}{(2K_1)^{3/2}}\times|A|^2-\Delta\omega\sqrt{2}-\frac{i}{\sqrt{2}\omega_0 Q}\right]A=F_0V_{dc}V_{ac} \quad (15)$$

with

$$F_0=\frac{\epsilon_0 wd}{Mh^2} \quad \Delta\omega=\omega-\omega_0. \quad (16)$$

Introducing $J=|A|^2$ and normalizing both sides, we obtain after simplification

$$J^3-J^2\frac{2\sqrt{2}\Delta\omega}{\gamma}+J\left(\frac{2\Delta\omega^2}{\gamma^2}+\frac{1}{2\omega_0^2Q^2\gamma^2}\right)-\frac{(F_0V_{dc}V_{ac})^2}{\gamma^2}=0 \quad (17)$$

with

$$\gamma=\frac{3K_3}{(2K_1)^{3/2}}. \quad (18)$$

This is a cubic equation of the form $J^3+C_2J^2+C_1J+C_0=0$. Constructing the constants

$$R=\frac{C_2^2-3C_1}{9}, \quad S=\frac{2C_2^3-9C_2C_1+27C_0}{54},$$
$$\Theta=\arccos(S/\sqrt{R^3}) \quad (19)$$

when $S^2-R^3>0$, Eq. (17) has one real solution

$$J=-\mathrm{sgn}(S)\left[(\sqrt{S^2-R^3}+|S|)^{1/3}+\frac{R}{(\sqrt{S^2-R^3}+|S|)^{1/3}}\right]$$
$$-\frac{C_2}{3}. \quad (20)$$

When $S^2-R^3\leq 0$, then Eq. (17) has three real roots

$$J_1=-2\sqrt{R}\cos\left(\frac{\Theta}{3}\right)-\frac{C_2}{3},$$
$$J_2=-2\sqrt{R}\cos\left(\frac{\Theta+2\pi}{3}\right)-\frac{C_2}{3}, \quad (21)$$
$$J_3=-2\sqrt{R}\cos\left(\frac{\Theta+4\pi}{3}\right)-\frac{C_2}{3}.$$

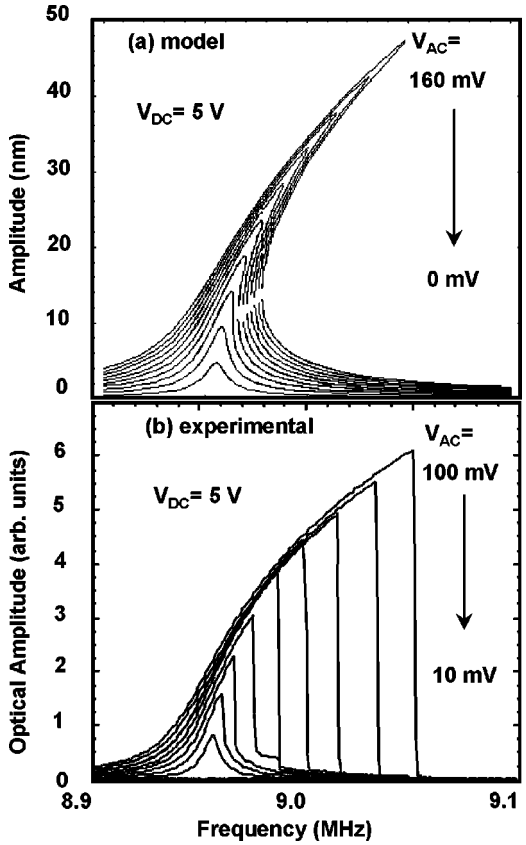


FIG. 6. Modeling and experimental observation of onset of nonlinearity of translational motion.

The presence of three real roots reflects the hysteretic shape of the nonlinear response, as some points on the frequency axis hold three solutions for the amplitude [Fig. 6(a)].

An important variable lies in the choice of Young's modulus. This modulus depends on the orientation and thickness of Si. It can also be affected by the presence of the contact metals or affected during processing. An effective value of Young's modulus is experimentally determined from the resonant frequency $f_0=8.96$ MHz of this structure. Taking the contact metal mass into account, we extract from Eq. (6) a value of $E_{exp}=87$ GPa. This experimental value is 1.5 to 2 times lower than the $E_{Si}=130-180$ GPa reported in the literature.[22,23] This apparent device softness is further discussed later. A quality factor of $Q=960$ is experimentally determined from the width of the symmetric peaks.

The resulting experimental and theoretical curves for a device of $d=3$ $\mu$m are shown in Fig. 6. For $V_{dc}=5$ V, the model reaches the critical amplitude at $V_{ac}=35$ mV. The experimental data reveal an onset of nonlinearity at $V_{ac}=10-20$ mV, in relative agreement with the order of magnitude predicted by the model. The model also predicts a peak amplitude of 15 nm under these drive conditions. As evidenced by the strong signal to noise ratio, signals two orders of magnitude smaller are still routinely detected, suggesting our ability to resolve angstrom-scale motion.[16]

## V. CHARACTERIZATION OF TORSIONAL MOTION

Given our interest in mesoscopic magnetometry,[3] we are mostly interested in the excitation and characterization of the torsional oscillation. This model begins with an equation of angular motion

$$I\ddot{\theta}+\kappa\theta+\frac{I}{\omega_0 Q}\dot{\theta}=\tau(\omega t,\theta), \tag{22}$$

where $I$ is the inertia of the paddle, and $\kappa$ is the combined torsional restoring constant of both Si wires. Mechanical nonlinear effects are not included given their absence from experimental results. The intrinsic resonant frequency of the torsional motion is given by

$$f_0=\frac{1}{2\pi}\sqrt{\frac{\kappa}{I}}=\sqrt{\frac{3}{\pi^2}\frac{\kappa}{\rho w a d^3}}, \tag{23}$$

where $\rho$ is the density of Si. The external torque is computed by solving the Coulomb equation for the electrostatic force, and by integrating over the area of the deflected paddle

$$\tau(\omega t,\theta)=\frac{\epsilon_0 V^2(\omega t)w}{2\theta^2}\left[\ln\left(\frac{h+d\sin\frac{\theta}{2}}{h-d\sin\frac{\theta}{2}}\right)+\frac{h}{h+d\sin\frac{\theta}{2}}-\frac{h}{h-d\sin\frac{\theta}{2}}\right]. \tag{24}$$

This expression has a removable singularity at the origin, and can be closely approximated by a third order expansion

$$\tau(\omega t,\theta)\approx-\epsilon_0 V^2(\omega t)w\left[\left(\frac{d^3}{12h^3}\right)\theta+\left(\frac{d^5}{40h^5}-\frac{d^3}{96h^3}\right)\theta^3\right]. \tag{25}$$

As it was the case for the translational mode, the torque depends on the square of the applied voltage, and a dc bias is added to force a linear term [Eq. (12)]. The equation of motion becomes

$$I\ddot{\theta}+\kappa\theta+\frac{I}{\omega_0 Q}\dot{\theta}=\alpha[V_{\rm dc}^2+2V_{\rm dc}V_{\rm ac}\sin(\omega t)+V_{\rm ac}^2\sin^2(\omega t)]\theta, \tag{26}$$

where

$$\alpha=\epsilon_0 w\frac{d^3}{12h^3}, \tag{27}$$

and where the cubic term in Eq. (25) has been neglected given the absence of noticeable experimental nonlinearity over the range of applied drive.

A rf signal at $\omega=\omega_0$ therefore contributes a strong torque at $\omega_0$ and a weak component at $2\omega_0$ through the crossed and squared ac terms, respectively. Equation (26) has the form of a damped Mathieu equation that has been previously employed to characterize parametric amplification effects in larger micromechanical systems.[13,14] First order perturbation theory predicts parametric resonances at drive frequencies of $\omega_d=2\omega_0/n$.[14] Although one could characterize the motion as combined parametric resonances of orders $n=1$, and $n=2$, our calculations suggest that uncontrolled asymmetries as small as 10 nm could also induce an angular independent torque and a significant linear torsional response under the range of applied drives. Nonetheless, evidence of $2\omega_0$ amplification has indeed been observed in this system, and these issues are currently under thorough investigation. Here we report the experimental observation of the first component of the right-hand drive term. We notice that the $V_{\rm dc}^2$ term acts as a dc perturbation in the effective torsional constant. This results in a perturbation of the observed resonant frequency

$$\frac{f_0'}{f_0}=\sqrt{1-\frac{\alpha}{\kappa}V_{\rm dc}^2}. \tag{28}$$

This perturbation has been observed as the bias is ramped from $V_{\rm dc}=0$ to 10 V for several paddle lengths [Fig. 7(a)]. The experimental data closely fits Eq. (28), providing values of the $\alpha/\kappa$ coefficient over a wide range of paddle lengths [Fig. 7(b)]. Figure 7(b) also verifies the expected cubic dependence of this coefficient [Eq. (27)]. Using the slope of this fit, and with $w=2\ \mu$m and $h=400$ nm, we find an experimental value of $\kappa_{\rm exp}=4.21\pm0.04\times10^{-12}$ N m.

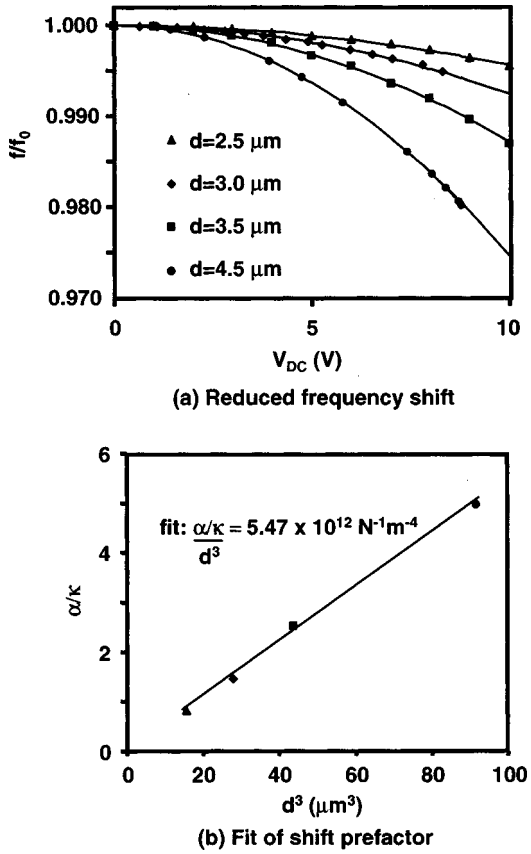


FIG. 7. Shift of resonant frequency with a dc bias for various paddle lengths. Shift parameter $\alpha/\kappa$ follows the expected cubic paddle length dependence. Fit of this parameter allows a precise evaluation of the effective torsional constant.

For macroscopic beams of rectangular cross sections, the torsional constant can be predicted using[24]

$$\kappa = 2\beta\left(\frac{a}{b}\right)\frac{ab^3}{L}G, \tag{29}$$

where $G_{Si}=6.7\times10^{10}\,\mathrm{Nm}^{-2}$ is the shear modulus of silicon, and $\beta(a/b)$ is a slowly varying dimensionless function of the ratio $b/a$. The factor of two takes the combination of both beams into account. With $\beta(1.14)=0.16$,[24] this macroscopic theory predicts $\kappa_{theo}=9.1\times10^{-12}\,\mathrm{N\,m}$. Experimental results suggest devices twice as soft as this theoretical prediction, in good agreement with the similar softness observed in the translational motion. This apparent softness could be the result of extensive crystalline damage during processing. However, additional experiments should be conducted in order to rule out other possibilities such as strain-induced artifacts.

## VI. CONCLUSION

We have reported the fabrication and characterization of paddle oscillators with nanometer scale supporting rods, resonant frequencies of 1–10 MHz, and $Q$ factors reaching $10^3$. Two modes of motion were observed, and have been experimentally identified as translational and torsional, respectively. We have presented a model of the electrostatic excitation and response of both modes. Analysis of translational and torsional results provides apparent values of Young's modulus of $E_{exp}=87\,\mathrm{GPa}$, and of the torsional constant of $\kappa_{exp}=4.21\pm0.04\times10^{-12}\,\mathrm{N\,m}$. Both values consistently suggest devices 1.5 to 2 times softer than expected from bulk silicon. Additional experiments are required to pinpoint the origin of this discrepancy. Significant nonlinearity is observed in the translational motion, and its onset theoretically predicted for vertical displacements greater than 15 nm. Evidence of parametric amplification has been observed, opening new possibilities for mesoscopic studies of such effects. We will also use these devices in mesoscopic temperature-dependent studies of loss mechanisms. Such devices offer great potential for small-scale studies of optical, magnetic, and mechanical phenomena.

## ACKNOWLEDGMENTS

The authors acknowledge the financial support of the NSF through the Cornell Center of Materials Research and the Cornell Nanofabrication facility. Fabrication of devices was performed at the Cornell Nanofabrication Facility. The authors thank Stephen W. P. Turner for several insightful discussions.

[1] C. Rossel, P. Bauer, D. Zech, J. Hofer, M. Willemin, and H. Keller, J. Appl. Phys. **79**, 8166 (1996); C. Rossel, M. Wileman, A. Gasser, H. Bothuizen, G. I. Meijer, and H. Keller, Rev. Sci. Instrum. **69**, 3199 (1998).
[2] P. A. Crowell, A. Madouri, M. Specht, G. Chaboussant, D. Mailly, and L. P. Levy, Rev. Sci. Instrum. **67**, 4161 (1996).
[3] R. D. Biggar and J. M. Parpia, Rev. Sci. Instrum. **69**, 3558 (1998).
[4] J. Morillo, Q. Su, B. Panchapakesan, M. Wuttig, and D. Novotny, Rev. Sci. Instrum. **69**, 3908 (1998).
[5] H. A. C. Tilmans, M. Elwenspoek, and J. H. J. Fluitman, Sens. Actuators A **30**, 35 (1992).
[6] G. Stemme, J. Micromech. Microeng. **1**, 113 (1991).
[7] A. Erbe, R. H. Bick, A. Tilke, A. Kriele, and J. P. Kotthaus, Appl. Phys. Lett. **73**, 3751 (1998).
[8] Z. Zhang, P. C. Hammel, M. Midzor, M. L. Roukes, and J. R. Childress, Appl. Phys. Lett. **73**, 2036 (1998); and references therein.
[9] J. A. Walker, K. W. Goossen, and S. C. Arney, J. Microelectromech. Syst. **5**, 45 (1996).
[10] H. Krommer, A. Erbe, A. Tilke, S. Manus, and R. H. Blick (unpublished).
[11] R. E. Mihailovich and N. C. MacDonald, Sens. Actuators A **50**, 199 (1995).
[12] T. S. Tighe, J. M. Worlock, and M. L. Roukes, Appl. Phys. Lett. **70**, 2687 (1997).
[13] D. Rugar and P. Grutter, Phys. Rev. Lett. **67**, 699 (1991).
[14] K. L. Turner, S. A. Miller, P. G. Hartwell, N. C. MacDonald, S. H. Strogatz, and S. G. Adams, Nature (London) **396**, 149 (1998).
[15] D. W. Carr, L. Sekaric, and H. G. Craighead, J. Vac. Sci. Technol. B **16**, 3821 (1998); D. W. Carr and H. G. Craighead, *ibid.* **15**, 2760 (1997).
[16] D. W. Carr, S. Evoy, L. Sekaric, J. M. Parpia, and H. G. Craighead, Appl. Phys. Lett. **75**, 920 (1999).
[17] A. N. Cleland and M. L. Roukes, Nature (London) **392**, 160 (1998).
[18] W. R. Wiszniewski, R. E. Collins, B. A. Pailthorpe, Sens. Actuators A **43**, 170 (1994).
[19] R. C. Weast, Ed., *Handbook of Chemistry and Physics*, 1st student ed. (CRC Press, Cleveland), p. F-51.
[20] M. S. Cheung, W. Li, S. E. Chidiac, *Finite Strip Analysis of Bridges* (E&FN SPON, London, 1996), p. 310.
[21] B. Yurke, D. S. Greywall, A. N. Pargellis, and P. A. Busch, Phys. Rev. A **51**, 4211 (1995).
[22] K. Petersen, Proc. IEEE **70**, 420 (1982).
[23] L. M. Zhang, D. Uttamchandi, and B. Culshaw, Sens. Actuators A **29**, 79 (1991).
[24] H. Ford, *Advanced Mechanics of Materials* (Longmans, Green, London, 1963).